Comparison of Airborne and Land-Based Radar Measurements of Precipitation during Winter MONEX[1]

R. A. HOUZE, JR.,[2] S. G. GEOTIS,[3] F. D. MARKS, JR.,[3] D. D. CHURCHILL[2] AND P. H. HERZEGH[4]

(Manuscript received 10 September 1980, in final form 14 March 1981)

ABSTRACT

The first quantitative test of the lower fuselage radar on the NOAA WP-3D aircraft was obtained during the Winter Monsoon Experiment (Winter MONEX). Reflectivities measured with this radar were compared with land-based measurements obtained with the MIT WR 73 weather radar, which was located on the north coast of Borneo for the experiment. Although the interpretation of the measurements with the WP-3D radar was difficult because of its wide vertical beam and the motion of the aircraft, the coverage of the MIT radar was fully three-dimensional and the volumes sampled by the WP-3D radar beam could thereby be placed into spatial context. The measurements with the two radar systems agreed to within 1–2 dB, excellent agreement for any two quantitative radars. Radar reflectivities computed from particle images obtained aboard the aircraft differed by only 2–3 dB from the aircraft radar measurements, again quite satisfactory agreement.

1. Introduction

Widespread scientific interest in the mesoscale organization of tropical and midlatitude precipitation systems has recently increased the need for quantitative radar observations worldwide. In many research and operational applications, airborne radar systems could fulfill this need more effectively than could stationary land-based radars. However, since airborne radar systems have not been widely available in the past, very little effort has been directed toward assessing their accuracy. Several factors such as beam width, antenna stability, and the horizontal motion of an aircraft with respect to precipitation areas around it can seriously affect the accuracy and interpretation of airborne radar measurements, and must be taken into account in the use of such measurements.

In the present study we assess the accuracy of reflectivity measurements obtained with a radar on the instrumented WP-3D aircraft of NOAA during the international Winter Monsoon Experiment (Greenfield and Krishnamurti, 1979). The WP-3D aircraft, called the P-3, which is equipped with weather radars in its nose, tail and lower fuselage, was based at Kuala Lumpur, on the Malay Peninsula (West Malaysia), and the WR 73 weather radar system of the Massachusetts Institute of Technology (MIT) was located at Bintulu, Sarawak, on the northern coast of Borneo (East Malaysia). On one of its research missions over the South China Sea, the P-3 flew within range of the MIT radar, allowing a comparison to be made between the echo patterns shown by the airborne and land-based radar systems. In this paper, we compare the quantitative reflectivity patterns obtained with the P-3 lower-fuselage radar and the MIT radar during this comparison flight. In a previous comparison, Jorgensen and Lewis[5] showed that the echo pattern obtained with the WP-3D lower fuselage radar in a hurricane was qualitatively consistent with the echo pattern shown by the WSR-57 radar of the National Weather Service in Brownsville, Texas.

2. Characteristics of the radar systems

Both the lower-fuselage radar of the P-3 and the MIT radar operate at 5 cm, and the signals of both radars are digitally processed. Characteristics of the systems are listed in Table 1. The digital processing of the aircraft radar is accomplished with a standard Digital Video Integrator Processor (DVIP). The MIT radar system uses an on-line minicomputer to control the direction of the antenna and to carry out all signal processing, averaging and recording

[1] Contribution No. 570, Department of Atmospheric Sciences, University of Washington.

[2] Department of Atmospheric Sciences, University of Washington, Seattle 98195.

[3] Department of Meteorology, Massachusetts Institute of Technology, Cambridge 02139.

[4] Center for the Environment and Man, Inc., Hartford, CT, 06120.

[5] Jorgensen, D., and B. M. Lewis, 1978: The precipitation structure of Hurricane Anita (1977) as revealed by quantized airborne radar. *Preprints 18th Conf. Radar Meteorology*, Amer. Meteor. Soc., 34–39.

0021-8952/81/070772-12$07.00

functions. The MIT radar has been calibrated and its performance monitored and controlled as described by Geotis (1975). Periodic calibrations with a signal generator provide continuing checks. From comparison measurements with other radars and with disdrometer measurements the standard error in measuring reflectivity is estimated to be approximately a decibel.

In addition to the characteristics listed in Table 1, the P-3 radar antenna is stabilized with respect to the pitch and roll of the aircraft, and the beam was usually tilted upward, typically at about 2.5°, to avoid echo from the ground. Further details of the P-3 weather radar systems can be found in the paper by Jorgensen and Lewis.

The MIT radar was used to obtain three-dimensional reflectivity patterns throughout the field phase of Winter MONEX. These patterns were obtained by running the antenna through a sequence of conical scans every 10 min, each sequence taking about 8 min to complete. This procedure was carried out from 7 December 1978 to 1 January 1979, providing a continuous record of the three-dimensional echo structure over the North Borneo coast and adjacent South China Sea region for almost a month. There were no significant interruptions in the data collection during this time.

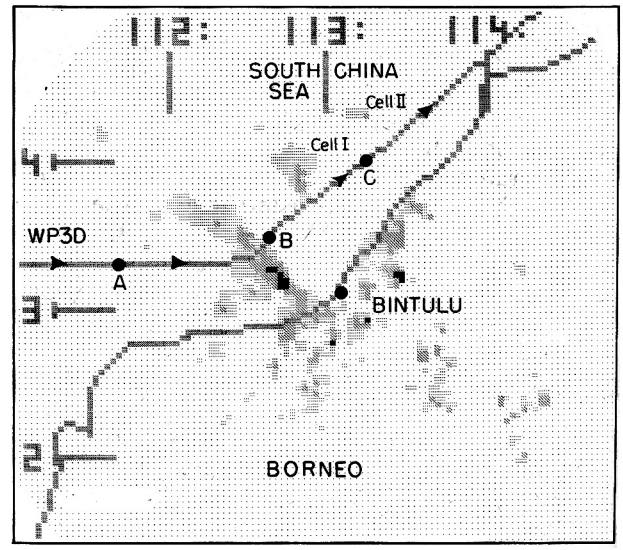

FIG. 1. Region of the intercomparison. Shaded circle is the area covered by the MIT radar located at Bintulu on the north coast of Borneo. Line with arrow shows the path of the NOAA WP-3D aircraft over the South China Sea. Intercomparison is made for the portions of the flight between A and B and B and C. The low-level radar echo pattern at 1430 LST 16 December 1978 (CAPPI for 2 km altitude inside 170 km range) from the MIT radar is shown. Thresholds for the echo shadings are 15, 30 and 40 dBZ.

3. Geographical and meteorological setting for the comparison

The path of the P-3 aircraft through the region of coverage of the MIT radar during the flight of 16 December 1978 is indicated in Fig. 1. Detailed comparisons of the echo patterns from the two radars for the flight path segments AB and BC are shown in the next section. Along AB, the aircraft approached and penetrated a line of convective echoes extending northwestward from the Borneo radar site. Between B and C, the aircraft passed two convective cells (I and II in Fig. 1).

The aircraft was flying at an altitude of 6.8 km, beneath an extensive layer of stratiform cloud.

TABLE 1. Radar system characteristics.

	MIT WR 73 radar	WP-3D aircraft lower fuselage radar
Wavelength (cm)	5.30	5.59
Pulse length (m)	300	900
PRF (s^{-1})	250	200
Peak power (kW)	250	70
Horizontal beamwidth (deg)	1.45	1.1
Vertical beamwidth (deg)	1.45	4.1
Azimuth averaging interval (deg)	1.0	1.8
Azimuth recording interval (deg)	1.0	0.5
Range bin size (km)	0.25–1.0	1.44
Maximum range recorded (km)	256	370

In satellite imagery, this cloud layer had the appearance of a large cirriform anvil, typical of equatorial latitudes. It was associated with convection that regularly forms along the Borneo coast at night during the winter monsoon. As this convection matures during the early morning hours, a widespread anvil develops. As the anvil widens, the precipitation from it becomes primarily stratiform. The anvil and its precipitation are usually located northwest of Bintulu and are best defined from 0400–0800 LST. After that time, the anvil and its precipitation generally move off to the west-northwest and dissipate.

By the time the aircraft was located at A, the upper level stratiform cloud layer, with some virga falling from it, was all that remained of this cloud system. The line of convection penetrated by the aircraft just before reaching B was a new development. The virga from the upper level anvil cloud was evaporating before reaching the surface and does not appear in the low-level echo pattern in Fig. 1. In subsequent figures, it will be seen that the virga appears in the echo patterns at higher levels on both the MIT and WP-3D radars.

4. Echo patterns detected with the airborne radar

A sequence of the echo patterns from the aircraft's lower fuselage radar are shown in Fig. 2. The virga from the dissipating anvil appears as a region of uniform echo, some 25 km × 60 km in dimension,

just north of the aircraft in Fig. 2a. The horizontally uniform appearance of the virga is characteristic of the stratiform anvil precipitation associated with the nocturnal cloud system.

At this time, the line of convection to the east of the aircraft was just becoming evident. The strong cellular echo at the southeastern end of the line, composed mostly of echo of 25–30 dBZ, was clearly seen, with two smaller, weaker echoes to its northwest, between the cellular echo and the region of virga. As the aircraft approached, the full line became detectable (Figs. 2b–2e). Except for the cells at its southeast end, the echo line was composed of fairly weak echo, generally around 20 dBZ. At the time of Fig. 2a, most of this weaker echo was below minimum detectable intensity. As the distance between the aircraft and the band decreased, the detectable portion of the line quickly increased. The substantial change in appearance of the convective echo line between Figs. 2a and 2c occurred over a time interval of only 4 min. This change illustrates how rapidly the appearance of the airborne radar echo pattern can change from one of isolated cells to one of an organized mesoscale line.

As the aircraft moved toward the convective line, the echo from the virga falling from the anvil decreased quickly in size (Figs. 2a–2d). By the time of Fig. 2e, the region of virga had disappeared. This change was partly an effect of the aircraft moving away from the echo. The virga did not extend very far below the aircraft's flight level and it probably filled a rapidly decreasing fraction of the 4.1° vertical beam width of the radar as the aircraft moved away. The change in the appearance of the virga, however, was at least partly real. The MIT radar data confirm that the region of virga was diminishing in size and intensity and actually disappeared between 1420 and 1440 LST.

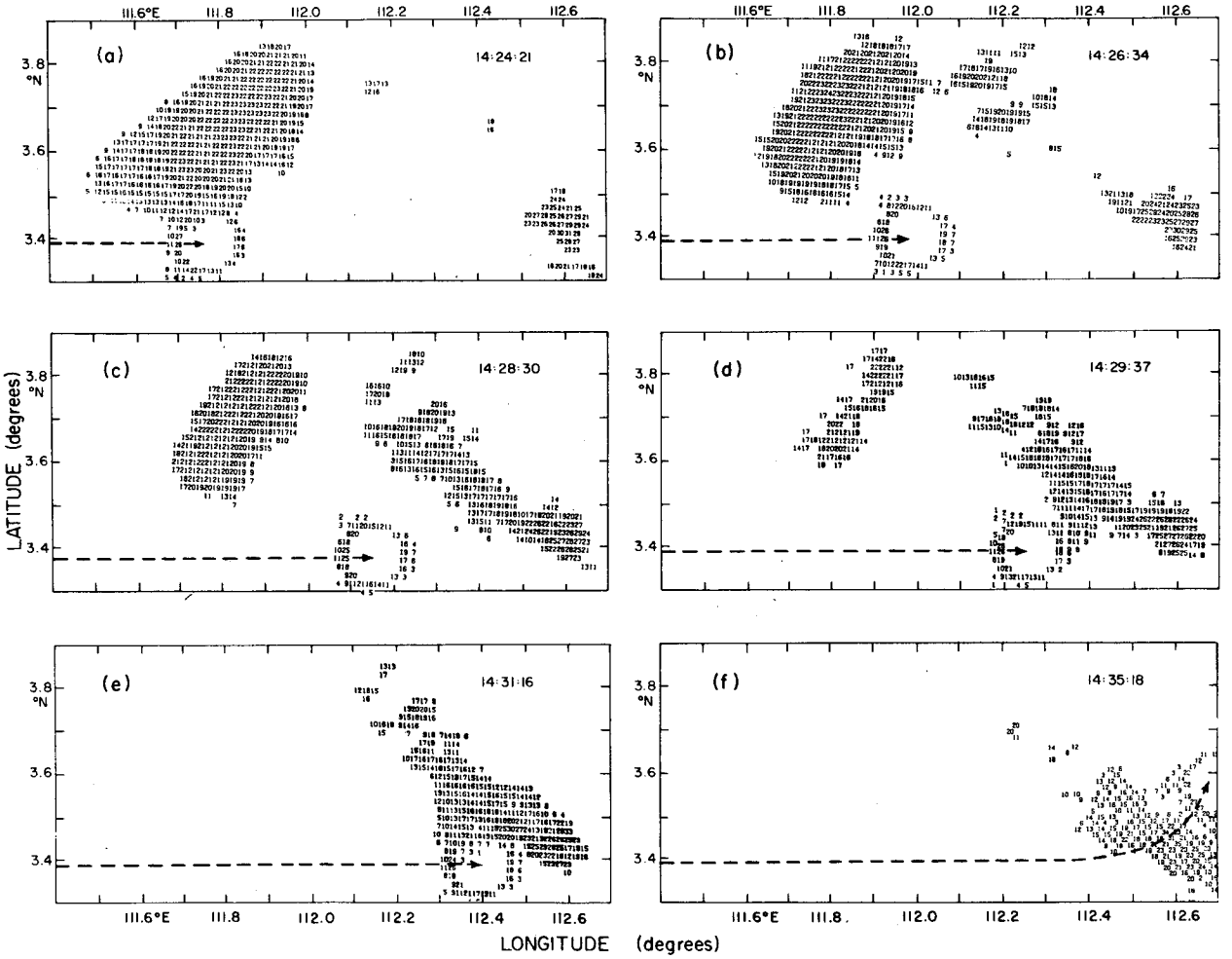

FIG. 2. Sequence of echo patterns shown by the lower fuselage radar of the WP-3D aircraft. Circle of echo around aircraft is from sea surface. Reflectivity values are in dBZ.

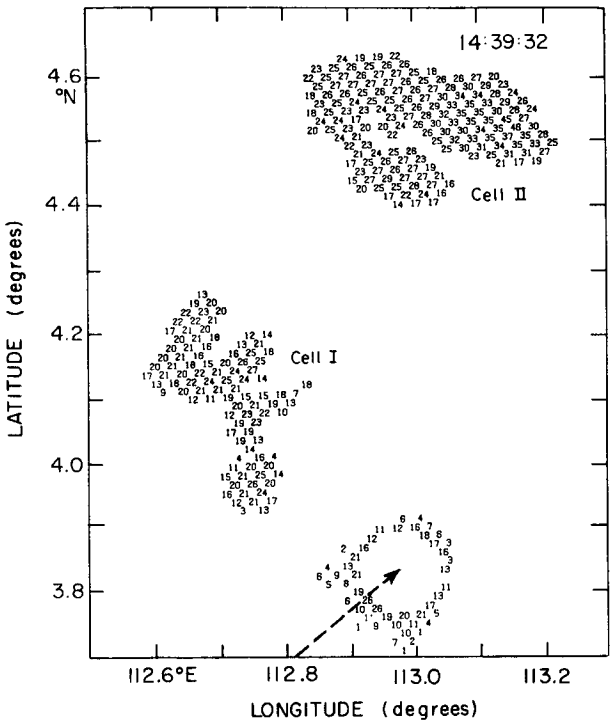

FIG. 3. Echo pattern of aircraft radar covering a geographical area to the northeast of that in Fig. 2.

The convective echo line was penetrated by the aircraft between 1433 and 1435 in the region of the strong cellular echo in the southeastern end of the line where a peak updraft speed of 5 ms^{-1} was encountered. The flight level temperature was −9°C and the liquid water content (measured by a Johnson-Williams probe) reached only 0.11 gm^{-3} even though the precipitation particles (sensed by a Particle Measuring System 2-D probe) in the 0.05–1.6 mm size range were predominantly lumps of graupel. The presence of graupel indicates the probable existence of considerably larger quantities of liquid water at an earlier stage or at another altitude in the cell. The echo pattern just after the penetration is shown in Fig. 2f. The pattern a few minutes later, as the aircraft passed cells I and II, is shown in Fig. 3.

5. Echo patterns detected with the land-based radar

The echo pattern from the MIT radar at Bintulu (Fig. 4) contained the same features as were seen in the radar echo pattern of the P-3 aircraft. In Fig. 4 and also in some of the later figures there are rather obvious data gaps in the maps. They are caused by some of the grid points (from which the CAPPI maps are constructed) being missed at the longer

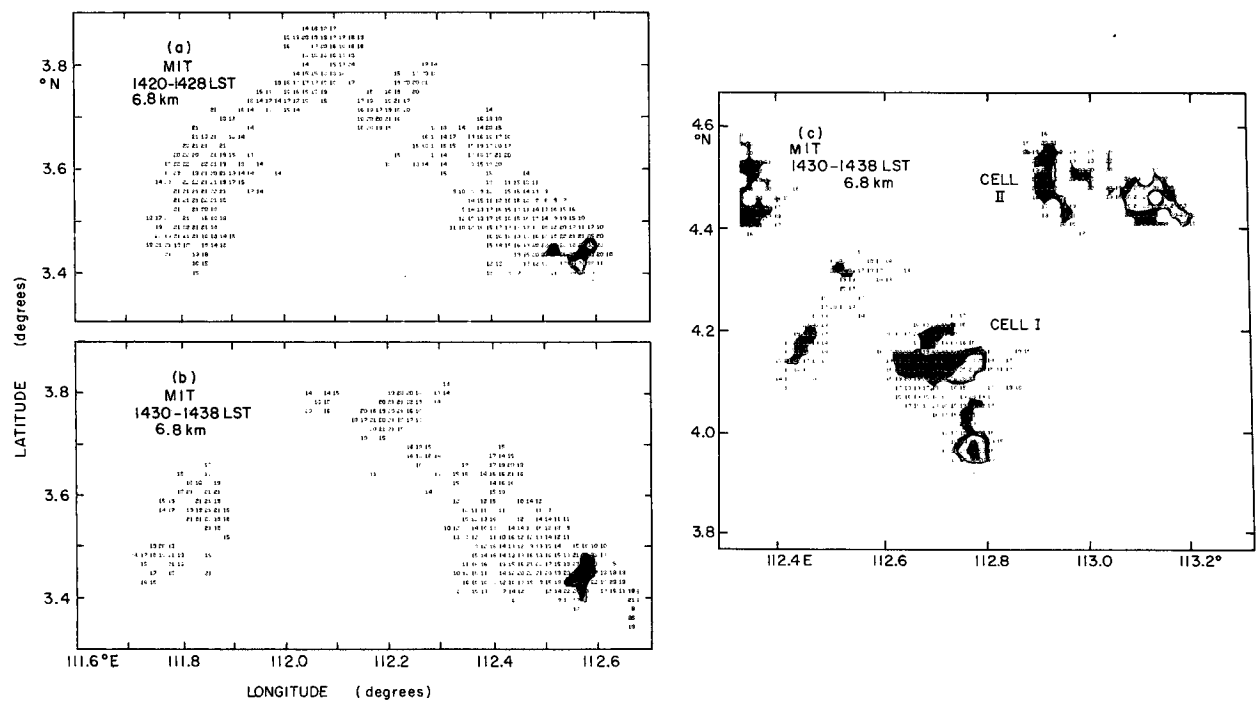

FIG. 4. Echo patterns for the 6.8 km level shown by the MIT land-based radar. Echo contours are drawn from 2 km × 2 km × 2 km resolution data for 24 and 30 dBZ. Patterns are constructed from the three-dimensional scans for 1420–1428 LST and 1430–1438 LST. Reflectivity values are in dBZ.

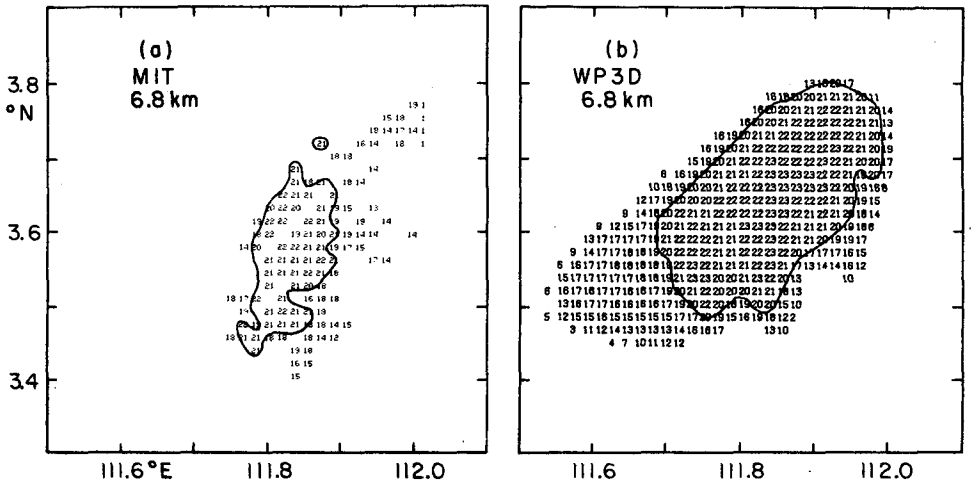

FIG. 5. Radar reflectivity patterns in anvil precipitation. Constant altitude (CAPPI) map from MIT radar for 6.8 km is shown in (a). Horizontal and vertical resolution is 2 km. The CAPPI is constructed from data collected between 1420 and 1428 LST. WP-3D lower fuselage radar data obtained at flight level 6.8 km at 14:24:21 LST are shown in 2 km horizontal resolution in (b). Contours are at 20 dBZ.

ranges where the vertical separation between successive conical scans exceeds the 2 km spacing of the grid.

In Fig. 4a, the virga from the anvil cloud is seen near 3.6°N, 111.8°E, and the convective line extends from 3.4°N, 112.6°E to 3.9°N, 112.0°E (compare with the P-3 pattern in Fig. 2c). Comparison of Figs. 4a and 4b shows the weakening of the virga which took place during that time. Cells I and II are seen in Fig. 4c (compare with Fig. 3).

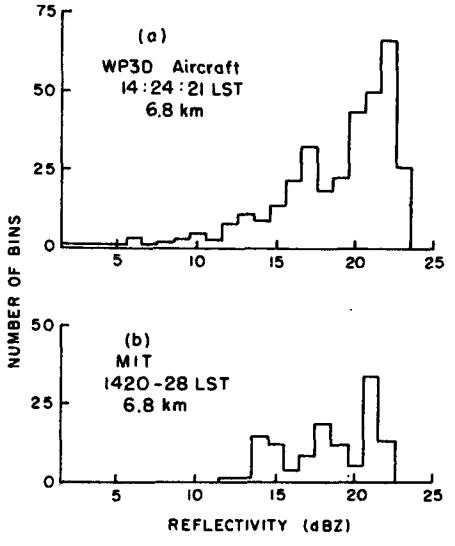

FIG. 6. Frequency of occurrence of reflectivities in 2 km × 2 km horizontal data bins in anvil precipitation as detected by WP-3D and MIT radars. Data are from Fig. 5.

6. Comparison of the airborne and land-based reflectivity measurements

a. Anvil precipitation

A detailed representation of the echo from the virga falling from the anvil (encountered along flight leg AB) is shown in Fig. 5a, a CAPPI map constructed from the three-dimensional scan obtained with the MIT land-based radar between 1420 and 1428 LST (same time as Fig. 4a). This map shows the virga at a height of 6.8 km, which corresponds to the aircraft's flight level. The horizontal and vertical resolution of the map is 2 km. The virga, as detected by the airborne radar at 1424 (same time as Fig. 2a) is shown in detail in Fig. 5b. The horizontal resolution of the map is 2 km, but the vertical resolution, determined by the 4.1° vertical beamwidth of the airborne radar, varies within the virga region from 0.5 km in the southern corner of the region (closest to the aircraft) to 3.5 km at its northern end (farthest from the aircraft).

The differences in vertical resolution between the two radars, the distance of the MIT radar from the echo (140 km) as compared to the proximity of the aircraft to the echo, and the fact that the MIT patterns are constructed from a lengthy (8 min) conical scan sequence obtained during a time when the echo was changing rapidly in time, all indicate that the horizontal distributions of reflectivity from the two radars cannot be expected to match in detail. However, it is reasonable to seek statistical agreement between the land-based and the airborne radar measurements. Fig. 6 shows that the re-

flectivity values from the two radars indeed have similar frequency distributions, with the airborne mean value being 22 dBZ while the land-based values were at 21 dBZ. Thus, we conclude that the two radars agreed to within ~1 dB in the reflectivity of the anvil precipitation. Better agreement could hardly be expected from the two radar systems. The lesser extent of the anvil echo, as sensed by the MIT radar (Fig. 5), is undoubtedly a result of the fact that much of the precipitation was too weak to be detected. The echo mass in the middle of the MIT pattern in Fig. 5a is centered within the strongest portion of the echo detected by the aircraft (Fig. 5b); however, the weaker fringes of the echo do not appear on the MIT radar pattern. At the range of this echo from the MIT radar, the minimum detectable signal is ~17 dBZ. From Figs. 5b and 6a it is clear that a sizable portion of the echo detected by the aircraft flying close to the echo was composed of echo weaker than 17 dBZ.

b. Convective line

The convective echo line penetrated by the aircraft along flight leg AB is shown in CAPPI maps for the MIT radar for the 6, 7 and 8 km levels in Fig. 7a–7c and in a detailed map from the airborne radar in Fig. 7d. The horizontal resolution of all of the maps is 2 km. The vertical resolution of the CAPPI maps is also 2 km. The vertical resolution of the aircraft map varies with distance from the aircraft, from about 0.5 km at the echo's closest point to the aircraft to about 3.5 km at its most distant point (northwest of the aircraft).

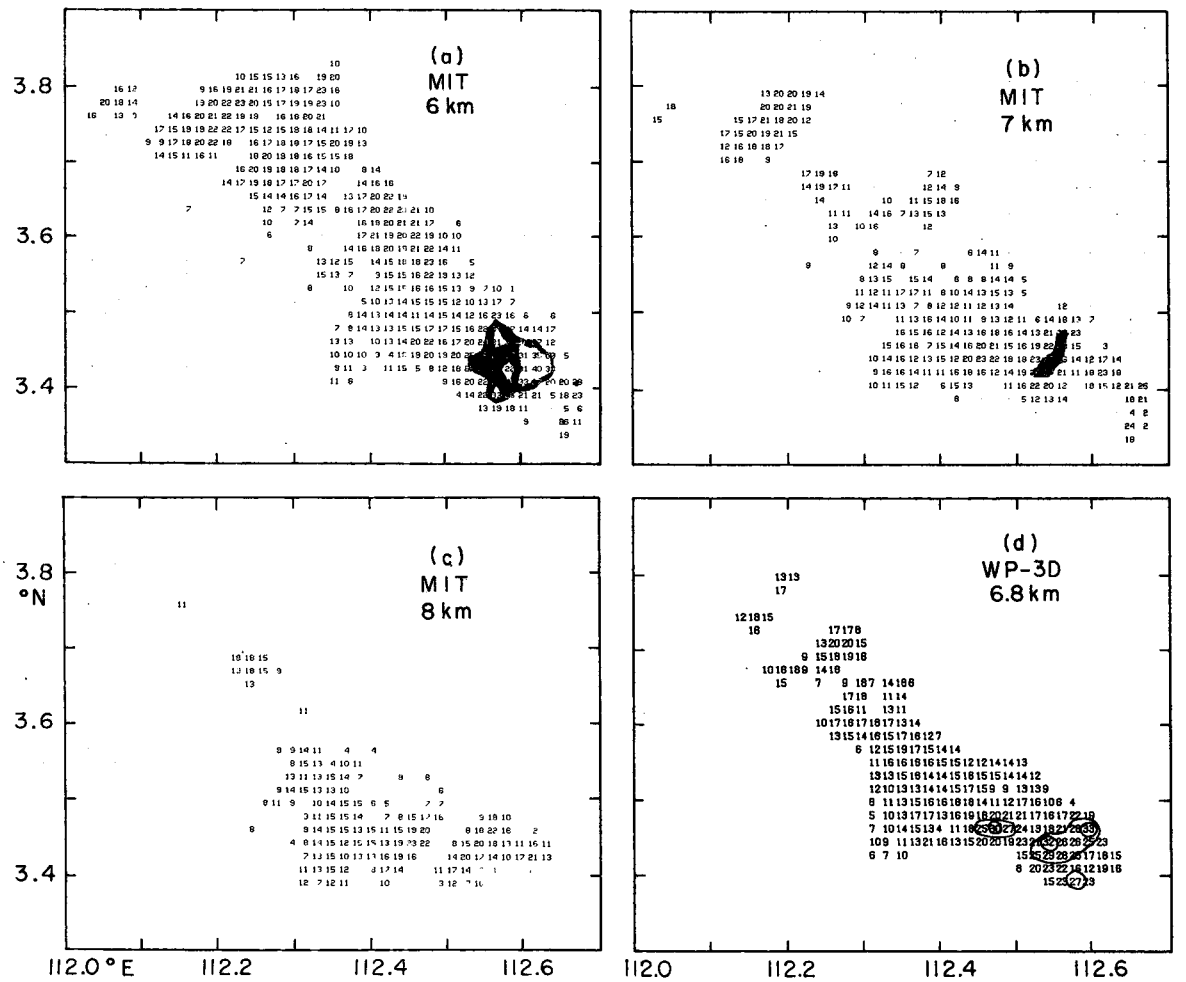

FIG. 7. Radar reflectivity patterns in the convective line. CAPPI maps from MIT radar are shown in (a)–(c). Horizontal and vertical resolutions are 2 km. CAPPI's are constructed from three-dimensional data collected between 1430 and 1438 LST. WP-3D lower fuselage radar data obtained at flight level 6.8 km at 14:31:16 LST are shown in 2 km horizontal resolution in (d). Contours are for 25 and 30 dBZ.

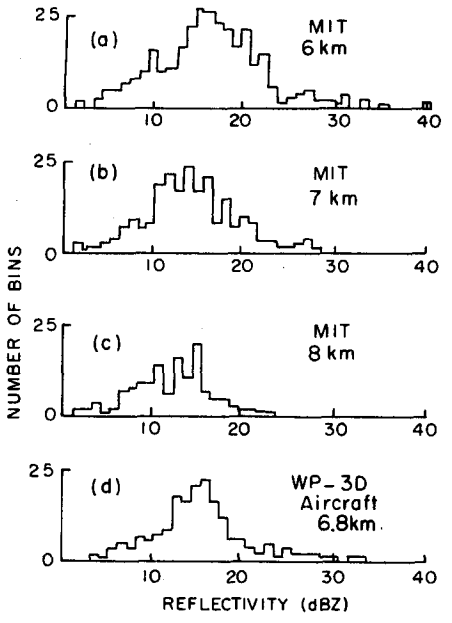

FIG. 8. Frequency of occurrence of reflectivities in 2 km × 2 km horizontal data bins in the convective line as detected by WP-3D and MIT radars. Data are from Fig. 7.

The line extended through a deeper layer of the atmosphere, changed its gross structure less rapidly in time, and was located nearer the MIT radar than the virga echo examined in the last section. Consequently, the patterns in the convective line echo detected by both radars, despite their different beam geometries and sampling schemes, were very similar in both size and detail. Comparison of Fig. 7b (the CAPPI corresponding closest in altitude to the flight level) and Fig. 7d shows good agreement between the airborne and land-based echo patterns in terms of the size and shape of the overall echo, the location of intense cellular regions within the general echo, and in the magnitudes of the reflectivities.

Reflectivity values are compared in Fig. 8, which shows frequency distributions of reflectivities in the convective line. The more varied texture of the convective line than that of the stratiform anvil precipitation gives these distributions greater spread and more symmetry than those associated with the virga (Fig. 6). Both the central value and spread of the frequency distribution for the airborne radar (Fig. 8d) lie between those of the 6 and 8 km CAPPI maps from the land-based radar (Figs. 8a and 8c), and the distribution for the CAPPI map corresponding most closely to flight level (7 km, Fig. 8c) is quite similar to the distribution for the airborne map. The mean value of the distribution for the airborne radar is 15.5 dBZ. This value is ~1 dB greater than the mean of the 7 km CAPPI curve, which is 14.7 dBZ. The mean values for the 6 and 8 km CAPPI curves of 16.2 and 12.5 dBZ, respectively, bracket the value for the airborne radar. Again, agreement between the two radar systems is quite satisfactory.

c. Convective cells

Along flight track segment BC, the aircraft approached to within 23 km of the edge of convective cell I (see Fig. 2). This echo was more than 100 km away from the land-based radar. The reflectivity pattern is shown in CAPPI maps from the land-based radar for the 5.8, 6.8 and 7.8 km levels in Figs. 9a–9c, and in the flight level map of the airborne radar in Fig. 9d. The horizontal resolution in all of these is 2 km × 2 km, and the vertical resolution in Figs. 9a–9c is again 2 km. Of course, the actual angular resolution of both radars increases with range but the effect is more important, for our considerations here, in the case of the airborne set because of its wide vertical beam. The vertical resolution of the aircraft's reflectivity pattern varies with distance from ~1.6 km, at the echo's nearest point to the aircraft, to 5.1 km at its furthermost point. Comparison of Figs. 9b and 9d shows the agreement of the shape of the echo pattern between the land-based and airborne radars. The weaker portions of the echo were below the minimum detectable intensity of the airborne radar; hence, the pattern detected by the land-based radar covered a larger area than did the airborne radar (approximately 544 km^2 vs 388 km^2). There is good agreement in the relative positions of regions of peak reflectivities, but the peak values in Fig. 9d are several decibels lower than corresponding values in Fig. 9b. There is better agreement, however, between the 6.8 km flight level radar map (Fig. 9d) and the 7.8 km CAPPI map (Fig. 9a). The overall shape is more similar, there is closer agreement in areal coverage between the two (444 km^2 vs 388 km^2), and near-matching of the peak reflectivity values. This can be explained by consideration of the elevation angle of the airborne radar. During the few seconds that the airborne radar was sweeping though this echo, the elevation angle of the beam was 2.6° above the horizontal. Consequently, the height of the center of the beam above sea level, at the nearest point of contact with the precipitation, was 8.0 km and, at the point of the echo furthest from the aircraft, 9.9 km.

Fig. 10 shows the frequency distribution of the reflectivity values found in Fig. 9. The mean value in Fig. 10d, corresponding to the airborne radar, is 18.2 dBZ. The mean value in Fig. 10a, corresponding to the 7.8 km level of the land-based radar, is

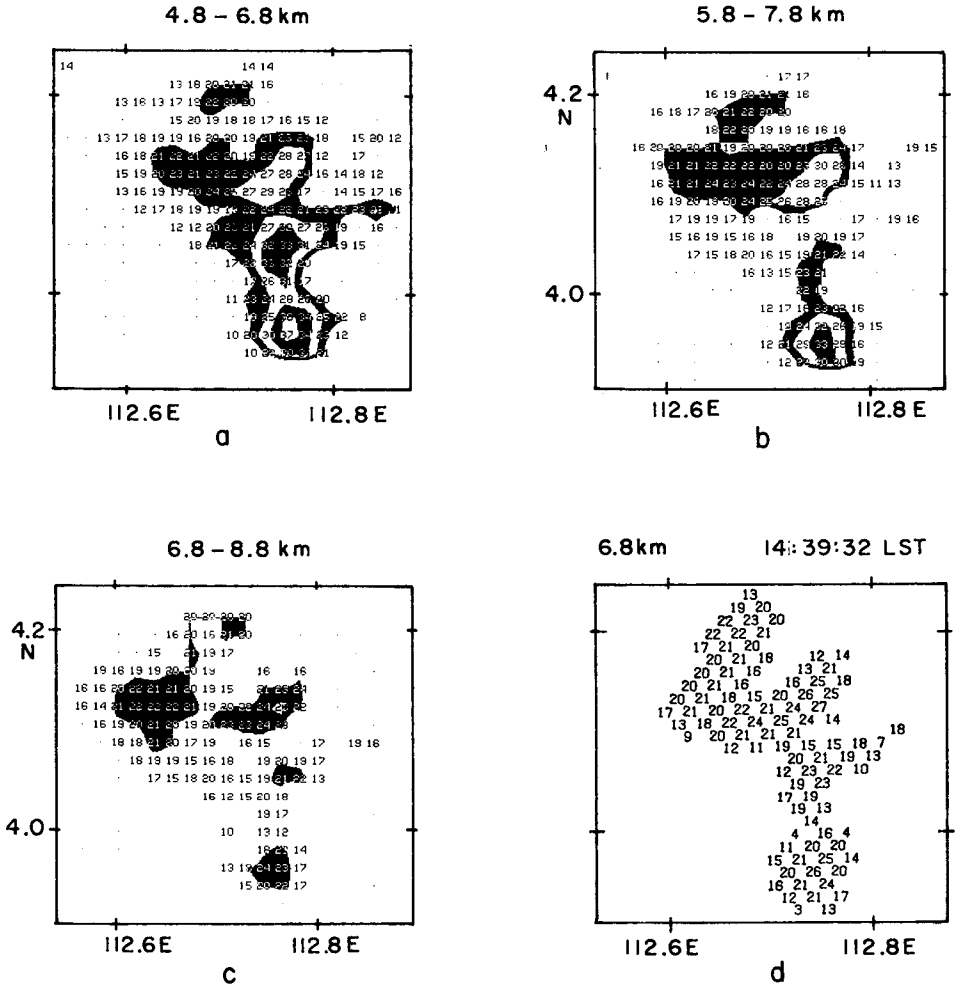

FIG. 9. Radar reflectivity patterns in cell I. CAPPI maps from MIT radar are shown in (a)–(c). Horizontal and vertical resolutions are 2 km. CAPPI's are constructed from three-dimensional data collected between 1430 and 1440 LST. WP-3D lower fuselage radar data obtained at flight level 6.8 km at 14:39:32 LST are shown in 2 km resolution in (d). Contours are for 20, 25 and 30 dBZ.

18.7 dBZ. Thus, the mean values agree to well within 1 dB, again very close agreement.

At 1445 LST, the aircraft approached to within 26 km of the southeastern edge of convective cell II (Fig. 3). The point of the echo closest to the land-based radar at this time was at a range of 132 km. Figs. 11a–11c show the CAPPI's for this region at 5.8, 6.8 and 7.8 km above sea level.

At this range, there are gaps in the data as a result of the process described in Section 5. No attempt was made to fill these gaps by automatic interpolation but the hand-drawn contours in Figs. 11a–11c probably indicate the actual reflectivity patterns reasonably well.

A detailed map of the reflectivities detected by the airborne radar is shown in Fig. 11d. The horizontal resolution in cell II is 2 km × 2 km, as in the CAPPI's while the vertical resolution increases from 1.8 km in the southeastern part of the cell to 4.7 km in its northwestern portion.

Between the two radars, there is qualitative agreement in the location of regions of peak reflectivity in cell II, and a general similarity in shape of the echo. However, the regions between the peak echoes of the land-based radar maps (Figs. 11a–1c) show little measurable reflectivity as a result of the high minimum detectable value (19 dBZ) for the land-based radar at this range, and gaps are seen in the data of the CAPPI maps at points where CAPPI values could not be determined as explained above.

The frequency distributions for the patterns in Fig. 11 are shown in Fig. 12. Each histogram for the land-based radar shows considerably less areal

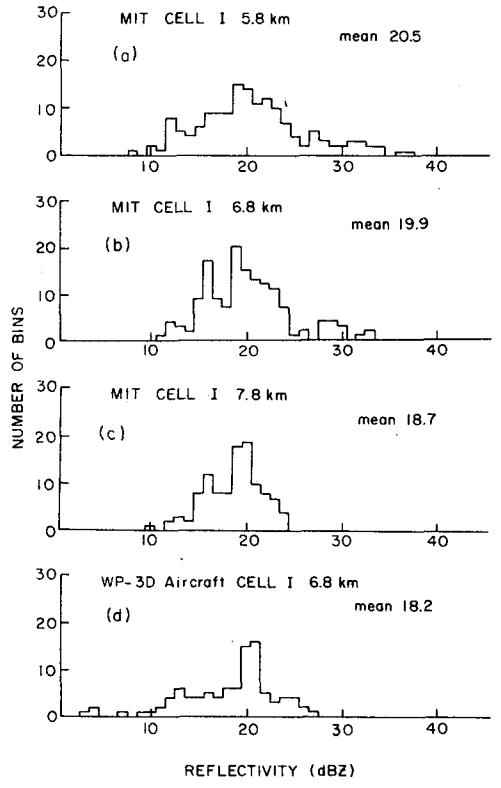

FIG. 10. Frequency of occurrence of reflectivities in 2 km × 2 km horizontal data bins in convective cell I, as detected by WP-3D and MIT radars. Data are from Fig. 9.

coverage than the airborne radar, for the reasons indicated. The former show a noticeable drop-off in the frequency of values below 18 dBZ, in agreement with the minimum detectable signal of the land-based radar at this range. In contrast, Fig. 12 shows numerous values below 18 dBZ for the airborne radar. In the region of the echo pattern in Fig. 11 where the largest values are observed, there are some gaps in the data of the CAPPI maps of Figs. 11a–11c. Consequently, Fig. 12d shows several occurrences of values > 30 dBZ which do not appear in the histograms for the land-based radar. Despite the limited sampling by the land-based radar at this range, the average reflectivity for the airborne radar of 22.8 determined from Fig. 12, is within 1 dB of the average value of 22.3 determined from the land-based radar's histogram corresponding in altitude most closely to the height of the center of the beam of the airborne radar.

7. Use of precipitation particle size distributions as a check on airborne radar measurements

A second method used to evaluate the accuracy of the WP-3D radar measurements was to compare the reflectivities obtained at flight level by this radar with reflectivities calculated from the size distributions of precipitation particles measured aboard the aircraft. Comparisons of this sort are particularly important since *in situ* measurements of particle size distributions will have to serve as the primary check on the WP-3D reflectivity measurements for periods in which no comparison with another quantitative radar is possible.

a. Processing of particle size distribution measurements

For the present study, size distributions of precipitation particles ≤ 1.6 mm in diameter were derived from digitized particle image data obtained by the Particle Measuring Systems (PMS) 2-D imaging probe (Model OAP-2D-C) aboard the P-3 aircraft [see Cannon (1976) for a discussion of the PMS imaging probes]. The particle image data were collected over 1.4 km path lengths during the penetration of the convective line echo shown in Figs. 2c–2f. Since the PMS probe only recorded the images of particles < 1.6 mm in diameter, it was necessary to extrapolate the derived size distributions in order to account for the presence of particles > 1.6 mm in diameter. Based on the observations of Houze *et al.* (1979) and Simpson and Wiggert (1971), it was assumed that the particle size distributions were exponential in form for diameters > 1.6 mm. Thus, our extrapolations in this diameter range followed the relation

$$N(D) = N_0 \exp(-\lambda D), \tag{1}$$

where $N(D)dD$ is the concentration of particles in the diameter range D to $D + dD$ and λ and N_0 are the slope and intercept of the distribution in logarithmic coordinates, respectively.

The values of λ used to extrapolate the particle size distribution measurements were based on the results of Houze *et al.* (1979), who showed that λ tends to vary inversely with temperature (T) in solid precipitation aloft in midlatitude frontal clouds. According to their $\lambda - T$ relationship, the mean value of λ for the particle size distributions measured at −9°C, the temperature at the flight level of the WP-3D aircraft during our comparison flight, should be ~1.7 mm^{-1}. Estimates of the upper and lower limits on the expected values of λ at −9°C were determined to be 1.5 and 1.9, the values which bound the 95% confidence interval for λ at that temperature for the data of Houze *et al.* (1979). Accordingly, the WP-3D particle size distribution measurements were extrapolated using values of λ ranging from 1.5 to 1.9 mm^{-1}.

The extrapolated size distributions were used to calculate values of radar reflectivity factor Z

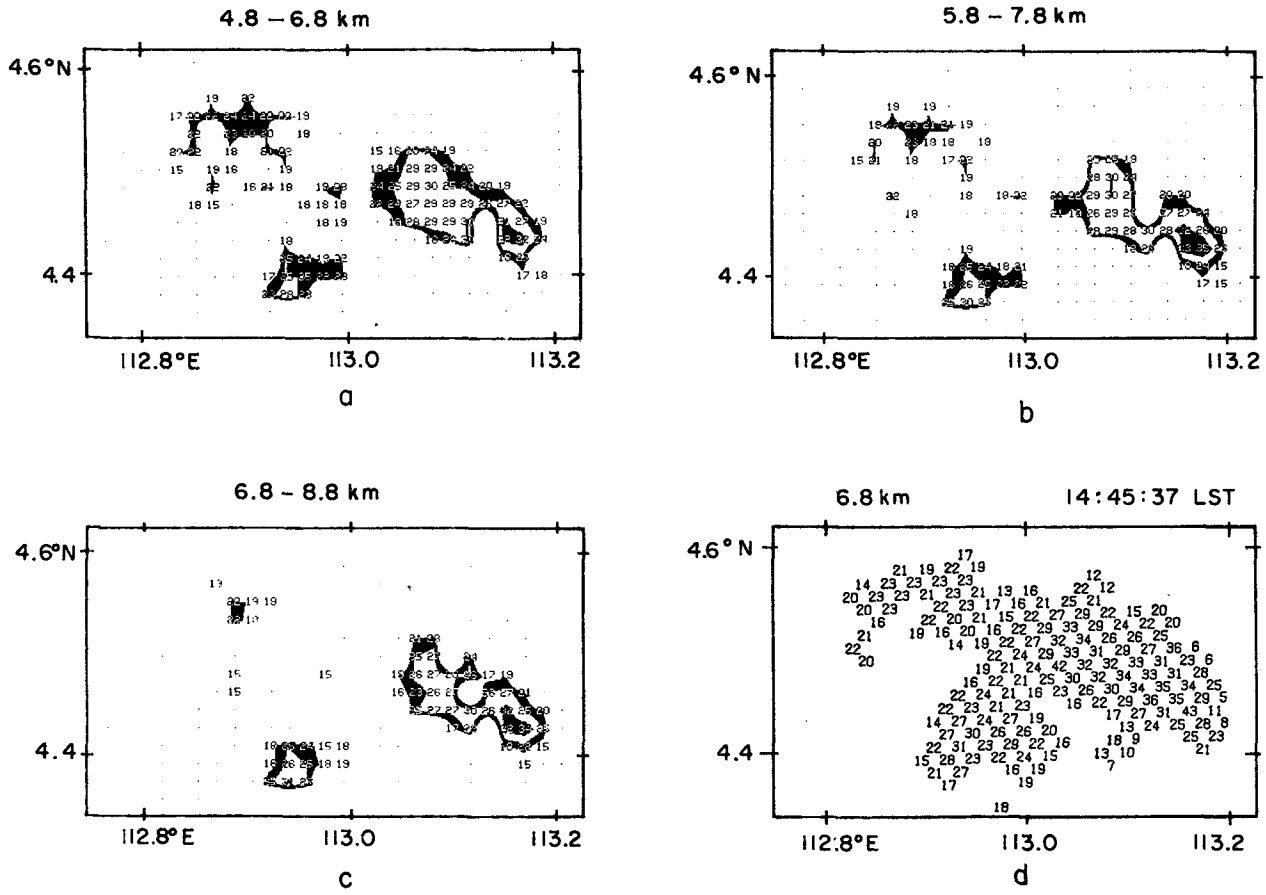

FIG. 11. Radar reflectivity patterns in cell II. CAPPI maps from MIT radar are shown in (a)–(c). Horizontal and vertical resolutions are 2 km. CAPPI's are constructed from three-dimensional data collected between 1440 and 1450 LST. WP-3D lower fuselage radar obtained at flight level 6.8 km at 14:45:37 LST are shown in 2 km resolution in (d), Contours are for 20, 25 and 30 dBZ.

($mm^6\ m^{-3}$) along the flight track of the WP-3D aircraft from the relation

$$Z = \sum_{i=1}^{L} N_i \delta_i D_i^6, \qquad (2)$$

where, N_i is the particle concentration per diameter interval (m^{-4}) for particles in size group i, δ_i is the interval (m) between the upper and lower bounds of size group i, D_i is the melted diameter of particles in size group i, and L indicates the largest size group for which $N_i \geq 10^2\ m^{-4}$. The values of D_i were calculated from the size and bulk density of the particles in each size group. The bulk densities used were based on the measurements of Locatelli and Hobbs (1974) and Knollenberg (1975).[6]

b. Comparison of calculated values of reflectivity factor with corresponding airborne radar measurements

The particles whose observed size distributions were used to calculate the reflectivity factor Z [from (2)] were in the form of ice, whereas reflectivities deduced from radar measurements are based on the assumption of scattering by water particles. Therefore, the radar-measured reflectivities must be adjusted for the difference in refractive index of water and ice, if the two types of measurements are to be compared. This adjustment results in an increase of 6.7 dB when the reflectivities from the flight-level measurements with the airborne radar are computed for ice instead of water.

The values of radar reflectivity for ice measured along the WP-3D flight track through the convective line were compiled to form the frequency histogram shown in Fig. 13a. This histogram compares favorably with that for the corresponding values of re-

[6] Knollenberg, R. G., 1975: The response of optical array spectrometers to ice and snow: A study of probe size to crystal mass relationships. Sci. Rep. No. 1, (SC175C) 141-9875-001, Air Force Cambridge Research Labs., 70 pp. [NTIS #AD-A 020 276].

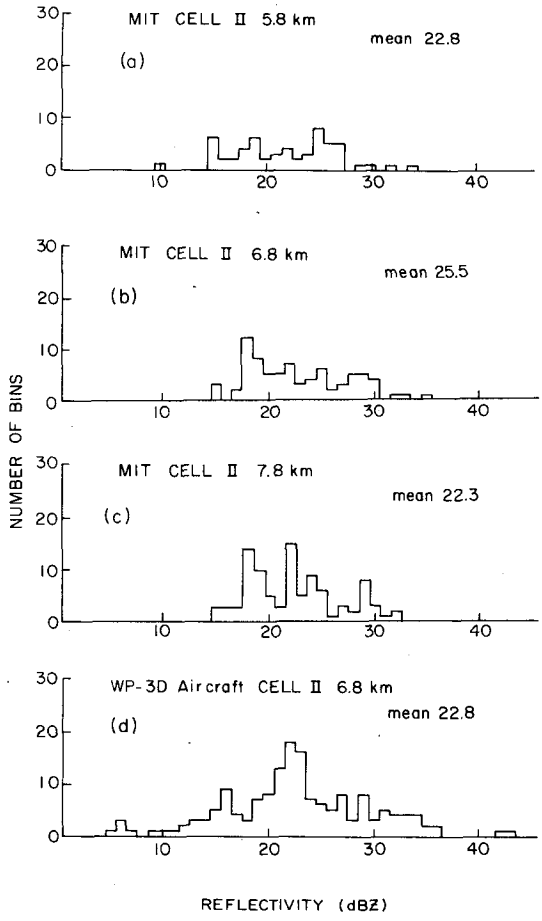

FIG. 12. Frequency of occurrence of reflectivities in 2 km × 2 km horizontal data bins in convective cell II, as detected by WP-3D and MIT radars. Data are from Fig. 11.

flectivity factor calculated from (2), which is shown in Fig. 13b. For example, the mean of the airborne radar measurements shown is 22.7 dBZ, while the mean of the calculated values is 25.3 dBZ. Given that the particle size distributions had to be extrapolated and that there are uncertainties in particle bulk density, natural variations in the particle size distributions and disparity in the volumes sampled by radar and the PMS probe, agreement within 2–3 dB as shown is about as good as can be expected. For reflectivity factors < 19 dBZ, the frequency of occurrence of calculated values is near zero, while that of the radar-measured values is significantly higher. This discrepancy is to be expected, since the process of extrapolation of the measured particle size distributions described in Section 7a cannot account for the occurrence of unexpectedly steep spectra which might be associated with low-reflectivity factors. In general, the reflectivity factors computed from particle size distributions measured along the flight track are consistent with the radar measurements.

8. Conclusions

The first quantitative test of the lower-fuselage radar system on the NOAA WP-3D has shown that the reflectivities measured by the WP-3D radar and the MIT WR73 weather radar system in two different types of echo features observed during Winter MONEX agree to within a decibel or two. Reasonable agreement was also obtained in comparisons between the reflectivities measured at flight level by the aircraft radar and those calculated from the size distributions of precipitation particles measured aboard the aircraft. These results indicate that the WP-3D radar measurements are accurate to within a few decibels, thus encouraging further quantitative use of WP-3D radar data.

Additional quantitative comparisons are necessary to determine, on a broader statistical basis, the accuracy and reliability of the WP-3D radar measurements. These comparisons can be made with any coastal or shipborne weather radar that is instrumented for digitally processing and recording reflectivity measurements and whose calibration is well-established. It is important, however, that the surface-based radar scan three-dimensionally in space, as the MIT radar did in the present study. Because of the large vertical beamwidth of the airborne radar, its vertical resolution decreases markedly with range. Real precipitation systems, such as those in the present study, often have

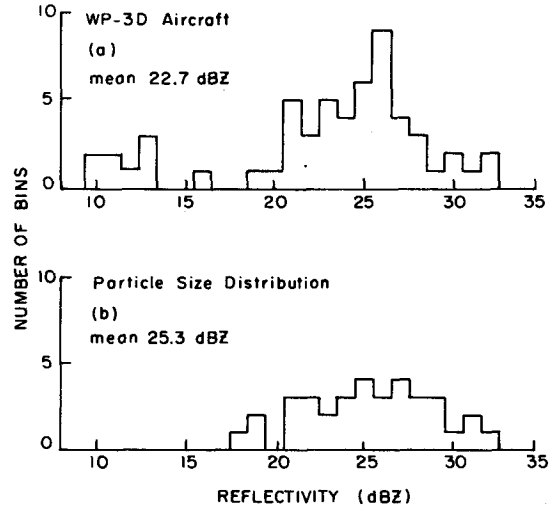

FIG. 13. Frequency of occurrence of reflectivities along the flight path through the convective line echo shown in Fig. 2f: (a) reflectivities measured by the WP-3D lower fuselage radar; (b) reflectivities calculated from particle size distribution measurements.

steep vertical gradients of reflectivity which when combined with the range-dependent vertical resolution of the airborne radar, give complicated reflectivity patterns. These effects are further complicated by the rapid motion of the aircraft, which can make the echo from an unchanging precipitation area undergo large changes in a matter of minutes. From the three-dimensional coverage of a surface-based radar, however, the reflectivity patterns shown by the airborne radar can be placed into spatial context and their quantitative consistency assessed.

Acknowledgments. The cooperation of the Airborne Mission Scientist, Dr. Peter J. Webster, and of the pilots and crew of the WP-3D aircraft made this study possible. The research was supported by the Global Atmospheric Program, Division of Atmospheric Sciences, National Science Foundation under Grant ATM78-00232.

REFERENCES

Cannon, T. W., 1976: Imaging devices. *Atmos. Tech.*, No. 8, 32–37.

Geotis, S. G., 1975: Radar as a quantitative weather instrument. *EASCON '75*, IEEE Publ. 75 Cho 998-5, 146 A–C.

Greenfield, R. S., and T. N. Krishnamurti, 1979: The Winter Monsoon Experiment—Report of December 1978 field phase. *Bull. Amer. Meteor. Soc.*, **60**, 439–444.

Houze, R. A., Jr., P. V. Hobbs, P. H. Herzegh and D. B. Parsons, 1979: Size distributions of precipitation particles in frontal clouds, *J. Atmos. Sci.*, **36**, 156–162.

Locatelli, J. D., and P. V. Hobbs, 1974: Fallspeeds and masses of solid precipitation particles. *J. Geophys. Res.*, **79**, 2185–2197.

Simpson, J. S., and V. Wiggert, 1971: 1968 Florida cumulus seeding experiment: Numerical model results. *Mon. Wea. Rev.*, **99**, 87–118.